arXiv:nucl-th/0111002v2 2 Nov 2001

Semi-classical Characters and Optical Model Description of Heavy Ion Scattering, Direct Reactions, and Fusion at Near-barrier Energies

B. T. Kim, W. Y. So, and S. W. Hong

Department of Physics and Institute of Basic Science, Sungkyunkwan University, Suwon 440-746, Korea

T. Udagawa

Department of Physics, University of Texas, Austin, Texas 78712

(February 8, 2008)

Abstract

An approach is proposed to calculate the direct reaction (DR) and fusion probabilities for heavy ion collisions at near-Coulomb-barrier energies as functions of the distance of closest approach D within the framework of the optical model that introduces two types of imaginary potentials, DR and fusion. The probabilities are calculated by using partial DR and fusion cross sections, together with the classical relations associated with the Coulomb trajectory. Such an approach makes it possible to analyze the data for angular distributions of the inclusive DR cross section, facilitating the determination of the radius parameters of the imaginary DR potential in a less ambiguous manner. Simultaneous χ^2-analyses are performed of relevant data for the ^{16}O+^{208}Pb system near the Coulomb-barrier energy.

24.10.-i, 24.10Eg, 25.70.Jj

Typeset using REVTEX

I. INTRODUCTION

Collisions between heavy ions at near-Coulomb-barrier energies are very much governed by the Coulomb potential involved, and thus the general features of the elastic scattering and direct reaction (DR) data can be understood based on the idea that the colliding ions primarily move along a classical Coulomb trajectory [1]. These features are seen most dramatically in plots of the ratios of the elastic differential cross section ($d\sigma_E/d\Omega$) or the inclusive (sum of all different) DR one ($d\sigma_D/d\Omega$) to the Rutherford differential cross section ($d\sigma_c/d\Omega$), *i.e.*,

$$P_i \equiv \frac{d\sigma_i}{d\Omega}/\frac{d\sigma_c}{d\Omega}\ (=\frac{d\sigma_i}{d\sigma_c}), \qquad (i = E \text{ or } D), \tag{1.1}$$

as a function of the distance of closest approach D (or the reduced distance d) [1,2] that is related to the scattering angle θ through

$$D = d(A_1^{1/3} + A_2^{1/3}) = \frac{1}{2}D_0\left(1 + \frac{1}{\sin(\theta/2)}\right) \qquad \text{with} \qquad D_0 = \frac{Z_1 Z_2 e^2}{E_{cm}}. \tag{1.2}$$

Here D_0 is the distance of closest approach in a head-on collision (s wave). Further, (A_1, Z_1) and (A_2, Z_2) are the mass and charge of the projectile and target ions, respectively, and E_{cm} (E_{lab}) is the incident energy in the center of mass (laboratory) system. P_E and P_D thus defined may be called the elastic and DR probabilities, respectively. The impact parameter b and orbital angular momentum ℓ, specifying the trajectory, are related to θ and D by

$$b = \frac{\ell}{k} = \frac{D_0}{2}\cot\frac{\theta}{2} = \sqrt{D(D - D_0)}, \tag{1.3}$$

where k is the wave number.

As an illustration, we show in Fig. 1 such plots of P_E and P_D for the ^{16}O+^{208}Pb system [3,4] at five different incident energies of E_{lab}=80, 84, 90, 96, and 102 MeV for P_E and at a single energy of E_{lab}=90 MeV for P_D, where the data are available. As seen, the values of P_E at different energies line up to form a very narrow band and take a value very close to unity for, say, $d > 1.65$ fm ($\equiv d_I$, interaction distance). When d becomes smaller than d_I, P_E falls off very rapidly, approximately exponentially.

The observed behaviour of P_E may easily be explained based on the physical picture that the projectile ion moves primarily along a Coulomb trajectory. For the case $d > d_I$, the trajectory is far away from the target and the projectile is scattered at the Coulomb scattering angle θ without being influenced at all by the nuclear force. The resultant scattering cross section is thus equal to the Rutherford cross section, and P_E becomes unity. When d becomes smaller than d_I, however, the incident ion gets under the influence of the strong nuclear interaction, and absorption takes place, reducing the P_E-value below unity.

In accordance with the observed behaviour of P_E, P_D starts to have a significant value at $d \approx d_I$. It reaches its maximum value ($P_D \approx 0.24$) at $d \approx 1.58$ fm, where P_E becomes approximately 0.7. In the region of $d = 1.58 \sim 1.65$ fm, the sum $P_E + P_D$ thus stays close to unity. This indicates that in that region, the main cause of absorption in the elastic channel is DR processes. When d becomes still smaller, the sum $P_E + P_D$ falls off rapidly from unity, showing that absorption due to more complicated processes eventually leading to fusion takes place. It is remarkable that the sum $P_E + P_D$ becomes extremely small, say, 10^{-3} and thus essentially zero, at around $d = d_c = 1.30$ fm, which is the distance for the s-wave Coulomb-barrier top. This means that the incident flux is almost completely absorbed when it reaches that distance. It is worth noting that the same picture holds irrespective of the incident energy, so long as it is not far away from the Coulomb-barrier energy.

Theoretically, we have a very well established optical model for evaluating P_E. This is not the case for P_D. There are a variety of theoretical methods that has been proposed for calculating contributions from inelastic scattering and transfer reaction processes to P_D by means of either semi-classical or classical approximations [1]. It is, however, still a formidable task to carry out calculations including all possible processes to obtain a theoretical value of P_D. The aim of the present work is to propose a simple approach to calculate P_D within the framework of an optical model that introduces two types of the imaginary potentials; one for DR, the other fusion [5–7]. We propose to evaluate P_D from the partial absorptive DR cross sections generated from the optical model calculation. The underlying assumption is that even after the reaction (removal from the elastic channel) the projectile ion still moves

along the Coulomb trajectory, being eventually emitted at the Coulomb scattering angle. Under the assumption, we may use the classical relation Eq. (1.3) to convert the partial wave cross section to P_D.

The same prescription may also apply to the partial fusion cross sections. This enables us to evaluate the hypothetical fusion probability P_F just as we calculate P_D. The conventional wisdom assumes [2] that

$$P_E + P_D + P_F \approx 1, \tag{1.4}$$

which expresses a simple physical idea that what is absorbed in the elastic channel at $r = D$ goes into either DR or fusion channels. Since there is no such measured P_F-value available, it has been impossible to test the above relation experimentally. However, it is possible to examine the relation by using the theoretical P_F. In the present work, theoretical expressions for P_D and P_F are derived in Sec. II, where we also perform numerical calculations of P_D and P_F along with P_E and examine the validity of the relation Eq. (1.4). The feasibility of evaluating P_D enables us to analyze the angular distribution of the inclusive DR cross section. This facilitates the determination of the DR part of the optical potential with less ambiguity. We shall demonstrate this also in Sec. II. In Sec. III, we repeat the simultaneous χ^2-analyses that we made several years ago [7] for the data on the ^{16}O+^{208}Pb system shown in Fig. 1. The reanalyses are needed since the fusion data have been revised [8] after Ref. [7] was published. Sec. IV will then be devoted to our conclusions.

II. OPTICAL MODEL CALCULATIONS OF P_D AND P_F

A. Derivation of Theoretical Expressions for P_D and P_F

In this subsection, we try to derive theoretical expressions for P_D and P_F within the framework of the optical model. We follow the approach proposed some time ago to calculate the total DR and fusion cross sections within the optical model by using imaginary, surface

type DR and volume type fusion, potentials, $W_D(r)$ and $W_F(r)$, respectively [5–7]. The total DR and fusion cross sections are then calculated as [9,10]

$$\sigma_i = \frac{2}{\hbar v} < \chi^{(+)} | W_i(r) | \chi^{(+)} > \qquad (i = D \text{ or } F), \tag{2.1}$$

where $\chi^{(+)}$ is the usual distorted wave function that satisfies the Schrödinger equation with the full optical model potential $U(r)$. σ_D and σ_F are thus calculated within the same framework as the differential elastic scattering cross section, $d\sigma_E/d\Omega$, is calculated. Such a unified description enables us to describe all different types of reactions on the same footing.

The basic ingredients for obtaining theoretical expressions for P_D and P_F are the partial wave cross sections, $\sigma_{i;\ell}$ ($i = D$ or F), which are obtained by simply expanding the cross sections, Eq. (2.1), into the partial wave components; $\sigma_i = \sum_\ell \sigma_{i;\ell}$. $\sigma_{i;\ell}$ can explicitly be given as [9]

$$\sigma_{i;\ell} = \frac{\pi}{k^2}(2\ell + 1) T_{i;\ell} \qquad (i = D \text{ or } F), \tag{2.2}$$

where

$$T_{i;\ell} = \frac{4}{\hbar v} \int_0^\infty |\chi_\ell(r)|^2 W_i(r) dr. \tag{2.3}$$

In the above equation, $\chi_\ell(r)$ is the partial distorted wave function and v is the relative velocity.

Eq. (2.2) with Eq. (2.3) is still a quantum mechanical expression, where ℓ takes only integer values. In what follows, we introduce a few semi-classical approximations customarily used [1,2,11,12]. The first is to treat ℓ as a continuous variable and to assume that

$$\frac{d\sigma_i(\ell)}{d\ell} = \sigma_{i;\ell}. \tag{2.4}$$

We then use the classical relation Eq. (1.3) that relates ℓ to θ. It is then straightforward to get

$$\frac{d\sigma_i(\ell)}{d\Omega} = \frac{1}{2\pi \sin\theta} \frac{d\ell}{d\theta} \frac{d\sigma_i(\ell)}{d\ell} = \frac{kD_0}{16\pi} \frac{1}{\cos(\theta/2)\sin^3(\theta/2)} \sigma_{i;\ell}. \tag{2.5}$$

Inserting further Eq.(2.2) into Eq.(2.5), and dividing the resultant expression by the Rutherford cross section σ_c, one finally obtains

$$P_i = \frac{2\ell+1}{kD_0}\tan(\theta/2)T_{i;\ell} \approx T_{i;\ell} \tag{2.6}$$

In obtaining the last expression, use is made of the approximation that $2\ell + 1 \approx 2\ell$.

In order that P_i can be a probability, it should satisfy

$$P_i \leq 1. \tag{2.7}$$

This requirement is indeed satisfied; in fact we have

$$P_D + P_F = T_{D;\ell} + T_{F;\ell} \equiv T_\ell = 1 - |S_\ell|^2, \tag{2.8}$$

where T_ℓ is the transmission factor and S_ℓ is the partial wave S-matrix. Since both P_D and P_F are positive quantities, it is clear from the above relation that P_D and P_F should be less than unity. (Note that there is no reason that P_E should be smaller than unity. Quantum effects such as interference and diffraction may cause the value to be greater than unity.) Now, for very small ℓ-values, we expect that $P_D \to 0$, hence

$$P_F \approx 1 - |S_\ell|^2 \to 1 \qquad \text{for small } \ \ell. \tag{2.9}$$

The last relation follows from the fact that for such a strong absorptive case as in heavy ion collisions, S_ℓ becomes essentially zero for small ℓ. Since $P_E + P_D \to 0$ for small ℓ, $P_E + P_D + P_F \to 1$ as expected earlier in Eq. (1.4). In the next subsection, we further study this point numerically.

In passing, we remark that the procedure we have proposed can also be used to reduce the quantum mechanical Rutherford cross section to the classical one. As is well known, this reduction has been given by using a set of semi-classical approximations [11,12]. The quantum mechanical Rutherford cross section has the well known form,

$$\frac{d\sigma_c}{d\Omega} = \left| \frac{1}{2ik} \sum_\ell (2\ell+1)(e^{2i\eta_\ell} - 1)P_\ell(\theta) \right|^2, \tag{2.10}$$

where η_ℓ is the Coulomb phase shift and P_ℓ is the Legendre function. One of the approximations introduced in the reduction process is to ignore the term $-\frac{1}{2ik}\sum_\ell(2\ell+1)P_\ell(\theta)$. This term gives rise to a divergent contribution at extremely forward angles and we ignore it as is usually done (see Refs. [11,12]). We then integrate Eq. (2.10) over angles to obtain the total elastic cross section expressed as a sum of the partial cross sections, which is in turn converted to an integral over ℓ. The resultant total elastic scattering cross section takes a very simple form, namely

$$\sigma_c = \sum_\ell \sigma_{c;\ell} = \int \frac{d\sigma_c}{d\ell} d\ell \quad \text{with} \quad \frac{d\sigma_c}{d\ell} = \sigma_{c;\ell} = \frac{\pi}{k^2}(2\ell+1) \approx \frac{\pi}{k^2}(2\ell). \tag{2.11}$$

By inserting the last expression in Eq. (2.11) into Eq. (2.5), we obtain the Rutherford differential cross section.

It appears that the procedure used for reducing the quantum mechanical Rutherford cross section to the classical one involves a contradictory element; we first integrate the differential cross section over angle, but then recover it from the partial wave cross sections we obtained as a result of the angle integration. However, the procedure can be justified: The quantum mechanical cross section Eq. (2.10) is given as a coherent sum over ℓ. As has been demonstrated in a number of semi-classical treatments of Eq. (2.10) [11,12], the dominant contribution to the differential cross section for a given scattering angle θ comes from the partial waves around $\ell = \ell_\theta$, where ℓ_θ is related to θ by Eq. (1.3). The contribution becomes δ-function-like in the classical limit of $\hbar \to 0$. In the present procedure, we carry out an integration over θ first, but from what has been discussed above, it is seen that the contribution from the angle θ is stored into the partial wave cross section of $\ell \approx \ell_\theta$. It is thus justifiable to recover the differential cross section at an angle θ from the partial wave cross section for $\ell = \ell_\theta$. This procedure is most justified when the scattering is closest to classical.

B. Numerical Examples

Calculations of P_E, P_D, and P_F are performed for the ^{16}O+^{208}Pb system with incident energy E_{lab}=90 MeV, using the optical model potential as fixed in our previous study [7]. We present the results in Fig. 2, where the solid, (thick and thin) dotted, and (thick and thin) dashed curves are the calculated values of P_E, P_D and P_F, respectively. The experimental data for P_E and P_D are also plotted by the solid and open circles, respectively. As seen, the calculated P_E reproduces the experimental P_E very well. This is not the case, however, for P_D; the calculated P_D is shifted to the smaller d-region by about 0.05 fm as compared with the experimental data, particularly in the region of $d \geq 1.6$ fm. Thus, the comparison of the calculated P_D with the data provides an additional test of the parameters used in Ref. [7]. In fact, this shift means the radius parameter $r_D = 1.50$ fm used in Ref. [7] is too small to describe the data. We thus repeated the calculation with a larger radius parameter of $r_D = 1.55$ fm. The calculated P_D thus obtained is plotted by the thin dotted curve shown in Fig. 2. The fit to the data is improved. It is worth noting that the recalculated P_D shifts toward the larger d-region by 0.05 fm, the same amount as the increase of the radius parameter r_D. This shows that the experimental P_D provides a very sensitive test of the r_D-value. Based on the result obtained above, we use the value r_D=1.55 fm in the χ^2-analysis discussed in the next section.

In the calculation of P_F shown in Fig. 2, use is made of r_F=1.40 fm. Thus the P_F curve lies in much smaller d-region than the P_D. We also observe that the slope of P_F is much steeper than that of P_D. This reflects the fact that the diffuseness parameter used for $W_F(r;E)$ (a_F=0.25 fm) is smaller than that of $W_D(r;E)$ ($a_D = 0.45$ fm). To show the effects of the a_F-value, we present by the thin dashed curve another P_F calculated with a_F=0.45 fm. It is seen that the slope of P_F at large distances is almost the same as that of P_D with $a_D = 0.45$ fm.

Let us now turn to the sum P_E+P_D+P_F shown by the dash-dotted curve. As expected, it stays very close to unity, confirming that the relation Eq. (1.4) is fairly well satisfied, within

the accuracy of, say, 20 %. The sum shows some oscillations around unity, which may be ascribed to quantum interference effects. The oscillation is also visible in the experimental P_E values. Accumulation of more accurate data may enable us to test this explanation in a more detailed manner.

Presented in Fig. 3 are the P_E-values calculated for the incident energies considered in Fig. 1. Use is made of the optical potential determined from the χ^2-analysis discussed in the next section. Since we use such a potential as determined from the χ^2-fit, the calculated P_E fit the data given in Fig. 1 very well and thus they forms a band very much similar to that seen in Fig. 1.

III. χ^2-ANALYSES

We have repeated simultaneous χ^2-analyses as in Ref. [7] for the elastic scattering, DR, and fusion data for the ^{16}O+^{208}Pb system. This is motivated for two reasons: The first is that the fusion data have been revised [8], after Ref. [7] was published. The second is that we are now able to test the calculations against the data for P_D. As described in the previous section, the value of the radius parameter r_D=1.50 fm used in Ref. [7] is too small to explain the data. A better r_D-value is r_D =1.55 fm. Other parameters must be fixed with this more appropriate value of r_D. As in Ref. [7], we utilize a dispersive type optical potential [13]

$$U = U_C(r) - [V_0(r) + V(r;E) + iW(r;E)], \tag{3.1}$$

where $U_C(r)$ is the Coulomb potential and $V_0(r)$ is the energy independent Hartree-Fock part of the potential, while $V(r;E) + iW(r;E)$ is the polarization part of the potential [14] that originates from couplings to reaction channels. They are assumed to have volume-type fusion and surface-derivative-type DR parts. Explicitly, $V_0(r)$, $V(r;E)$ and $W(r;E)$ are given, respectively, by

$$V_0(r) = V_0 f(X_0), \tag{3.2}$$

$$V(r;E) = V_F(r;E) + V_D(r;E) = V_F(E) f(X_F) + 4V_D(E) a_D \frac{df(X_D)}{dR_D}, \tag{3.3}$$

$$W(r;E) = W_F(r;E) + W_D(r;E) = W_F(E) f(X_F) + 4W_D(E) a_D \frac{df(X_D)}{dR_D}, \tag{3.4}$$

where $f(X_i) = [1 + \exp(X_i)]^{-1}$ with $X_i = (r - R_i)/a_i$ ($i = 0,\ D$ or F) is the usual Woods-Saxon function. Use is made of the values used in Ref. [7] for the parameters of the bare potential $V_0(r)$, and the geometrical parameters of $V(r;E)$ and $W(r;E)$ (except r_D as discussed above); V_0=60.4 MeV, r_0=1.176 fm, a_0=0.658 fm, r_F=1.40 fm, a_F=0.25 fm, r_D=1.55 fm, and a_D=0.45 fm. Once the geometrical parameters are fixed, the dispersion relation is reduced to a relation for the strength parameters $V_i(E)$ and $W_i(E)$ ($i = D$ and F). The relation now reads [13]

$$V_i(E) = V_i(E_s) + \frac{E - E_s}{\pi} P \int_0^\infty dE' \frac{W_i(E')}{(E' - E_s)(E' - E)}, \tag{3.5}$$

where P stands for the principal value and $V_i(E_s)$ is the potential value at a reference energy point $E = E_s$.

As was done in Ref. [7], we approximate the E-dependence of $W_i(E)$ just above the threshold energy $E_{0;i}$ (defined as $W_i(E_{0;i}) = 0$) by a linear function of E. (See the forthcoming Eqs. (3.7) and (3.8).) We then identify this threshold energy as that determined from the linear representation of the quantity $S_i(E)$ introduced by Stelson *et al.* [16] as

$$S_i \equiv \sqrt{E\sigma_i(E)} \propto (E - E_{0;i}) \qquad (i = D \text{ or } F). \tag{3.6}$$

The threshold energies $E_{0;i}$ thus defined are essentially the threshold energies of the DR ($i = D$) and fusion ($i = F$) cross sections, and it is plausible to identify the two threshold energies to be the same. The authors of Ref. [16] considered the quantity S_i only for the $i = F$ case, but we extend it to DR. Originally, two threshold phenomena in the imaginary part of the optical potential and the fusion cross section data were found independently, but it was noticed later [17] that the two are very close to one another. Once we have separated the imaginary potential into the DR and fusion parts, it is physically plausible to require

that the two thresholds should be the same. In Fig. 4, we present the S_i-values for $i = D$ and F. There we find that $E_{0;D}$ =73.0 MeV and $E_{0;F}$=76.0 MeV, which will be used later as the threshold energies of $W_D(E)$ and $W_F(E)$, respectively.

In an attempt to determine the polarization potential, simultaneous χ^2-analyses were performed, treating all four strength parameters, V_D, V_F, W_D and W_F as the adjustable parameters. We took into account all the data [3,4] available for incident energies between E_{lab}=80 MeV and 104 MeV. We included the total DR and fusion cross sections in the analyses.

The values of the parameters thus extracted are presented in Fig. 5 for V_D and W_D and in Fig. 6 for V_F and W_F. Let us consider first the results for V_D and W_D. A considerable fluctuation is seen in the values of V_D, but W_D changes smoothly as a function of E. The fact that W_D could be fixed as a smooth function of E indicates that these values are reliable. There is a reason that W_D can be determined rather unambiguously and becomes a smooth function of E. It is because W_D is the dominant absorptive term in the peripheral region. Therefore, the elastic scattering cross section is quite sensitive to the value of W_D. This is not the case for V_D; at the strong absorption radius, where the elastic scattering cross section is sensitive to the real potential, V_D is generally much smaller than the bare potential $V_0(r)$, resulting in difficulty in determining V_D unambiguously. The fluctuation seen in Fig. 5(a) may be understood to arise from this difficulty.

The W_D-values determined from the χ^2-analyses can be well represented by the following function of E (in units of MeV):

$$W_D(E) \;=\; \begin{cases} 0 & \text{for } E \leq 73.0 \\ 0.015(E-73.0) & \text{for } 73.0 < E \leq 92.5 \\ 0.2925 & \text{for } E > 92.5 \end{cases} \tag{3.7}$$

where $E_{0;D}$=73.0 MeV is used as extracted in Fig. 4. The solid line shown in Fig. 5(b) is W_D given by Eq. (3.7). The line fits the empirical values quite well.

Since a reliable value of W_D is now available, one can calculate V_D by using the dispersion relation Eq. (3.5). In doing this, we need to know one more parameter, *i.e.*, the value of

V_D at $E = E_s$. We may fix this $V_D(E_s)$ by fitting the average of the resultant V_D to that of the empirically determined V_D. The solid curve shown in Fig. 5(a) shows the V_D-values thus calculated. The $V_D(E_s)$-value used is $V_D(E_s)$=0.4 MeV at E_s=92.5 MeV.

As seen in Fig. 6, V_F and W_F are both determined as fairly smooth functions of E. The W_F-values may be represented (in units of MeV) as

$$W_F(E) = \begin{cases} 0 & \text{for } E \leq 76.0 \\ 0.32(E - 76.0) & \text{for } 76.0 < E \leq 86.0 \\ 3.2 & \text{for } E > 86.0 \ . \end{cases} \tag{3.8}$$

Again we took the threshold energy of $E_{0;F}$=76.0 MeV determined from S_F. The solid line shown in Fig. 6(b) represents W_F in Eq. (3.8). We then calculated the $V_F(E)$ by using the dispersion relation Eq. (3.5) with W_F given by Eq. (3.8). The reference potential $V_F(E_s)$ involved was chosen as $V_F(E_s)$=3.50 MeV at E_s=86.0 MeV. As shown by the solid curve in Fig. 6(a), the predicted V_F-values again agree reasonably well with the empirically determined values.

We take as our final potential parameters W_D and W_F given, respectively, by Eqs. (3.7) and (3.8), and also V_D and V_F generated from the dispersion relation Eq. (3.5). The potential with such parameters then fully satisfies the dispersion relation. Using such an optical potential, we calculated the final theoretical P_E, σ_D, and σ_F and presented them in Figs. 7 and 8 in comparison with the experimental data. As seen, all experimental P_E, σ_D and σ_F are well reproduced by the calculations.

We now wish to give some remarks on the polarization potential we obtained. First, there is a remarkable difference in the the energy dependences between the DR and fusion potentials. A very rapid change is seen only in the fusion part of the potential. The slope of $W_F(E)$ given by Eq. (3.8) in the threshold region is 0.32, while that in $W_D(E)$ given by Eq. (3.7) is only 0.015. As a result, we see a significant energy variation of about 2 MeV in $V_F(E)$ in the interval of $\sim$ 10 MeV, but the change in V_D is only 0.1 MeV in the energy range of $\sim$ 20 MeV. We may thus conclude that the threshold anomaly exists in the fusion part of the potential, but not in the DR part.

IV. CONCLUDING REMARKS

We have presented a simple method to calculate the DR and fusion probabilities within the optical model by introducing two types of imaginary potentials, DR and fusion. These probabilities are calculated by using the partial DR and fusion cross sections generated from the corresponding imaginary potentials with the help of the classical relation between the orbital angular momentum ℓ and the scattering angle θ. The probabilities thus calculated were shown to satisfy the condition that the value should be equal to or less than unity.

Based on the expressions derived, numerical calculations of these probability were performed. We found that the sum of the DR, fusion and elastic probabilities stays close to unity. We also analyzed the angular distribution data of the inclusive DR cross section, demonstrating that the data provide useful information for determining the radius parameters of the DR potential. It was observed that a very rapid energy variation (threshold anomaly) was in the fusion part of the potential, but it is hardly seen in the DR part, particularly in the real part of the potential.

A simultaneous χ^2-analysis of elastic scattering, DR and fusion cross sections for the ^{16}O+^{208}Pb system at near-barrier energies were performed for determining the polarization part of the optical potential that satisfies the dispersion relation over all space. The potential thus determined is found to reproduce the data well.

The authors wish to express their sincere thanks to Prof. W. R. Coker for his kind reading of the manuscript and comments. One of the authors (BTK) acknowledges the support by Korea Research Foundation (KRF-2000-DP0085).

REFERENCES

[1] R. Bass, *Nuclear Reactions with Heavy Ions* (Springer-Verlag, New York, 1980)

[2] G. R. Satchler, *Introduction to Nuclear Reactions* (John Wiley & Sons, New York, 1980) p.41.

[3] F. Videvaek *et al.*, Phys. Rev. C **15**, 954 (1977).

[4] E. Vulgaris, L. Gradzins, S. G .Steadman, and R. Ledoux, Phys. Rev. C **33**, 2017 (1986).

[5] S.-W. Hong, T. Udagawa, and T. Tamura, Nucl. Phys. **A491**, 492 (1989).

[6] T. Udagawa, T. Tamura, and B. T. Kim, Phys. Rev. C **39**, 1840 (1989).

[7] B. T. Kim, M. Naito, and T. Udagawa, Phys. Lett. B **237**, 19 (1990).

[8] C. R. Morton, A. C. Berriman, M. Dasgupta, D. J. Hinde, J. O. Newton, K. Hagino, and I. J. Thompson, Phys. Rev. C **60**, 044608 (1999).

[9] T. Udagawa and T. Tamura, Phys. Rev. C **29**, 1922 (1984); T. Udagawa, B. T. Kim, and T. Tamura, Phys. Rev. C **32**, 124 (1985).

[10] M. S. Hussein, Phys. Rev. C **30**, 1962 (1984).

[11] N. F. Mott and H. S. W. Massey, *The Theory of Atomic Collisions*, (Oxford University Press, 1965) p.97-102.

[12] K. W. Ford and J. A. Wheeler, Ann. Phys. **7**, 287 (1959).

[13] C. Mahaux, H. Ngo, and G. R. Satchler, Nucl. Phys. **A449**, 354 (1986); Nucl. Phys. **A456**, 134 (1986); M. A. Nagarajan, C. Mahaux, and G. R. Satchler, Phys. Rev. Lett. **54**, 1136 (1985).

[14] W. G. Love, T. Terasawa, and G. R. Satchler, Nucl. Phys. **A291**, 183 (1977).

[15] G. R. Satchler, M. A. Nagarajan, J. S. Lilley, and I. J. Thompson, Ann. of Phys. **178**, 110 (1987).

[16] P. H. Stelson, Phys. Lett. B **205**, 190 (1988); P. H. Stelson, H. J. Kim, M. Beckerman,

D. Shapira, and R. L. Robinson, Phys. Rev. C **41**, 1584 (1990).

[17] T. Udagawa, M. Naito, and B. T. Kim, Phys. Rev. C **45**, 876 (1992).

FIGURE CAPTIONS

Fig. 1. The experimental elastic probabilities, P_E, as a function of the reduced distance D for the ^{16}O+^{208}Pb system at E_{lab} = 80, 84, 90, 96, and 102 MeV. The measured DR probabilities, P_D, are also plotted at E_{lab} = 90 MeV. The data are taken from Refs. 3 and 4.

Fig. 2. The optical model predictions of elastic, DR, and fusion probabilities as a function of the reduced distance D for the ^{16}O+^{208}Pb system at E_{lab} = 90 MeV are shown in comparison with the experimental ones. The theoretical total probabilities are also shown. The thick dotted curve denotes P_D calculated with the dispersive optical potential determined in Ref. 7. The thin dotted curve represents P_D calculated with the same potential but with modified r_D (=1.55 fm). The thick (thin) dashed curve denotes P_F calculated with $a_F = 0.25$ fm ($a_F = 0.45$ fm).

Fig. 3. The results of calculations for elastic probabilities, P_E, as a function of the reduced distance D for the ^{16}O+^{208}Pb system at E_{lab} = 80, 84, 90, 96, and 102 MeV, using the final fully dispersive optical potential.

Fig. 4. The Stelson plot of $S_i = \sqrt{E_{cm}\sigma_i}$ for direct reaction ($i = D$, solid circles) and fusion ($i = F$, open circles) cross sections. The straight lines are drawn to show the extraction of the threshold energies. Thin lines connecting the circles are only to guide the eyes.

Fig. 5. The strength parameters $V_D(E)$ and $W_D(E)$ for the direct reaction potential as functions of E. The open and solid circles are the values extracted from the χ^2-analyses. The solid lines denote $W_D(E)$ and $V_D(E)$ calculated, respectively, from Eq. (3.7) and from Eq. (3.5) together with Eq. (3.7). The thin lines connecting the circles are only to guide the eyes.

Fig. 6. The strength parameters $V_F(E)$ and $W_F(E)$ for the fusion potential as functions of E. The open and solid circles are the values extracted from the χ^2-analyses. The solid lines denote $W_F(E)$ and $V_F(E)$ calculated, respectively, with Eq. (3.8) and Eq. (3.5). The thin lines are to guide the eyes.

Fig. 7. The ratios of the elastic scattering cross sections to Rutherford cross sections calculated with our final optical potential for the ^{16}O+^{208}Pb system are shown in comparison with the experimental data. The data are taken from Refs. 3 and 4.

Fig. 8. The direct reaction and fusion cross sections calculated with our final optical potential for the ^{16}O+^{208}Pb system are shown in comparison with the experimental data. The direct reaction data are taken from Refs. 3 and 4, while the fusion ones from Ref. 8.

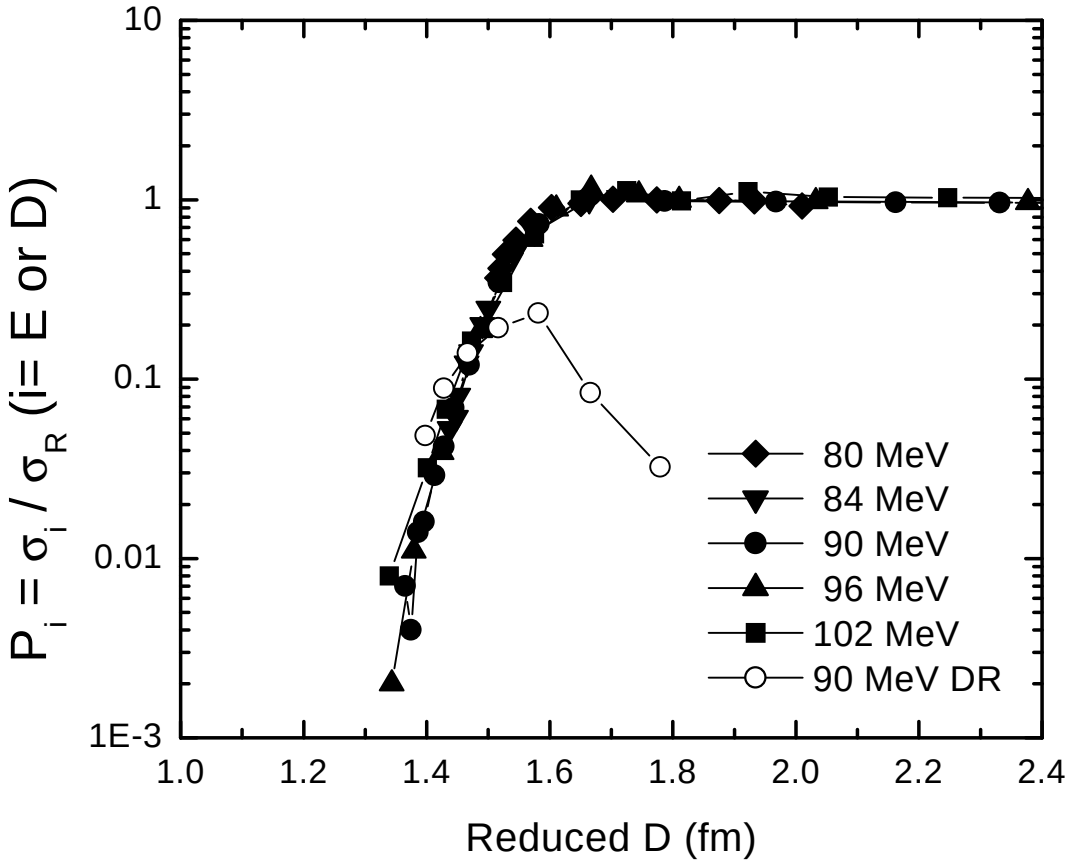
10
1
0.1
0.01
1E-3
1.0
1.2
1.4
1.6
1.8
2.0
2.2
2.4
$P_i = \sigma_i / \sigma_R$ (i= E or D)
Reduced D (fm)
80 MeV
84 MeV
90 MeV
96 MeV
102 MeV
90 MeV DR

Fig. 1

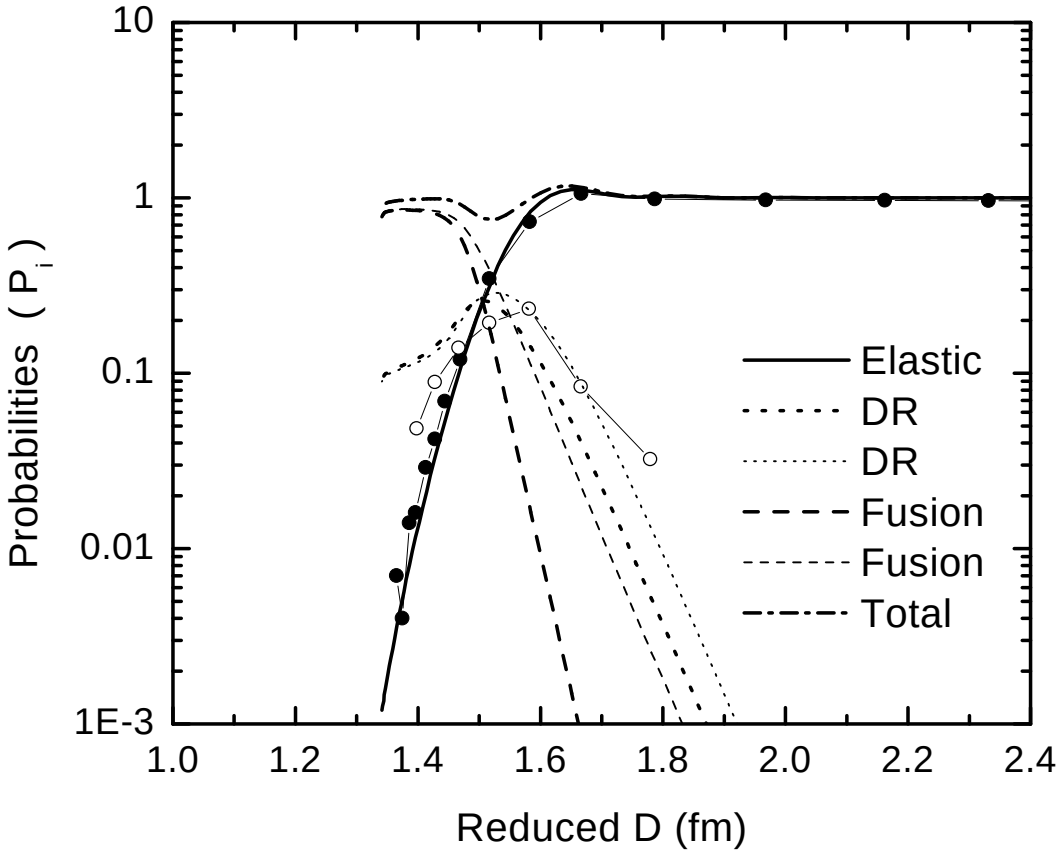
10
1
0.1
0.01
1E-3
Probabilities (P_i)
1.0
1.2
1.4
1.6
1.8
2.0
2.2
2.4
Reduced D (fm)
Elastic
DR
DR
Fusion
Fusion
Total

Fig. 2

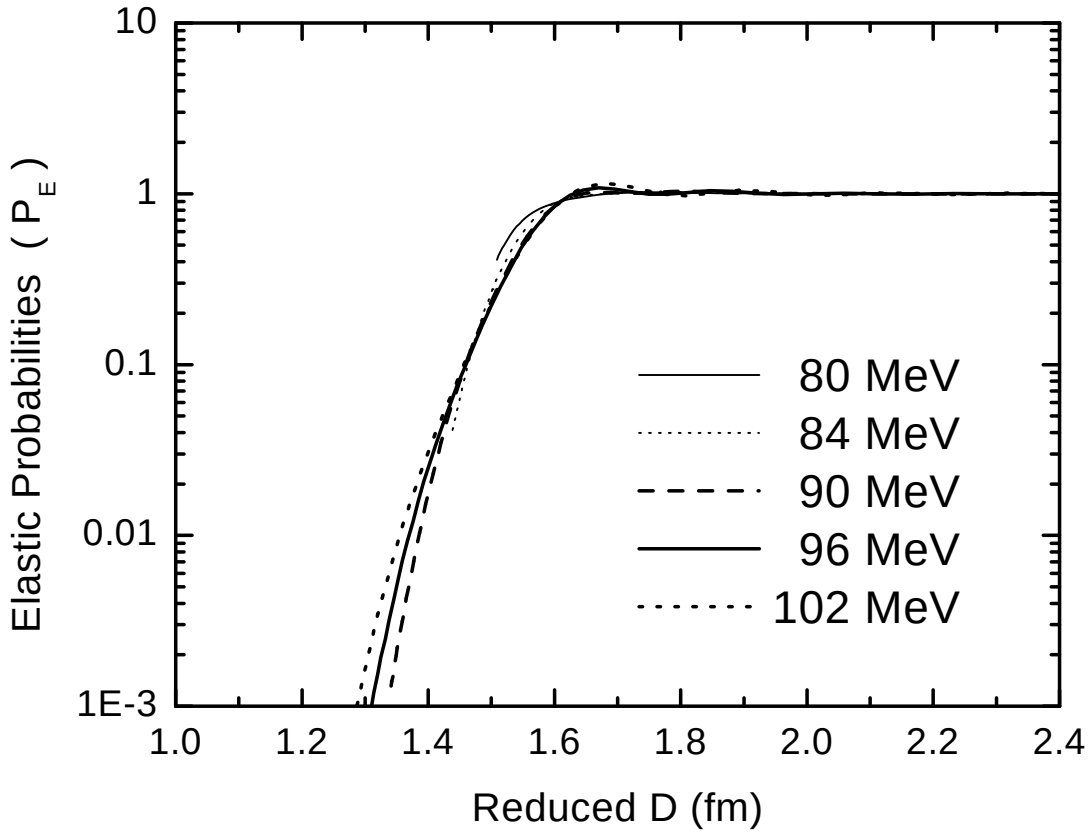
10
1
0.1
0.01
1E-3
Elastic Probabilities (P_E)
1.0
1.2
1.4
1.6
1.8
2.0
2.2
2.4
Reduced D (fm)
80 MeV
84 MeV
90 MeV
96 MeV
102 MeV

Fig. 3

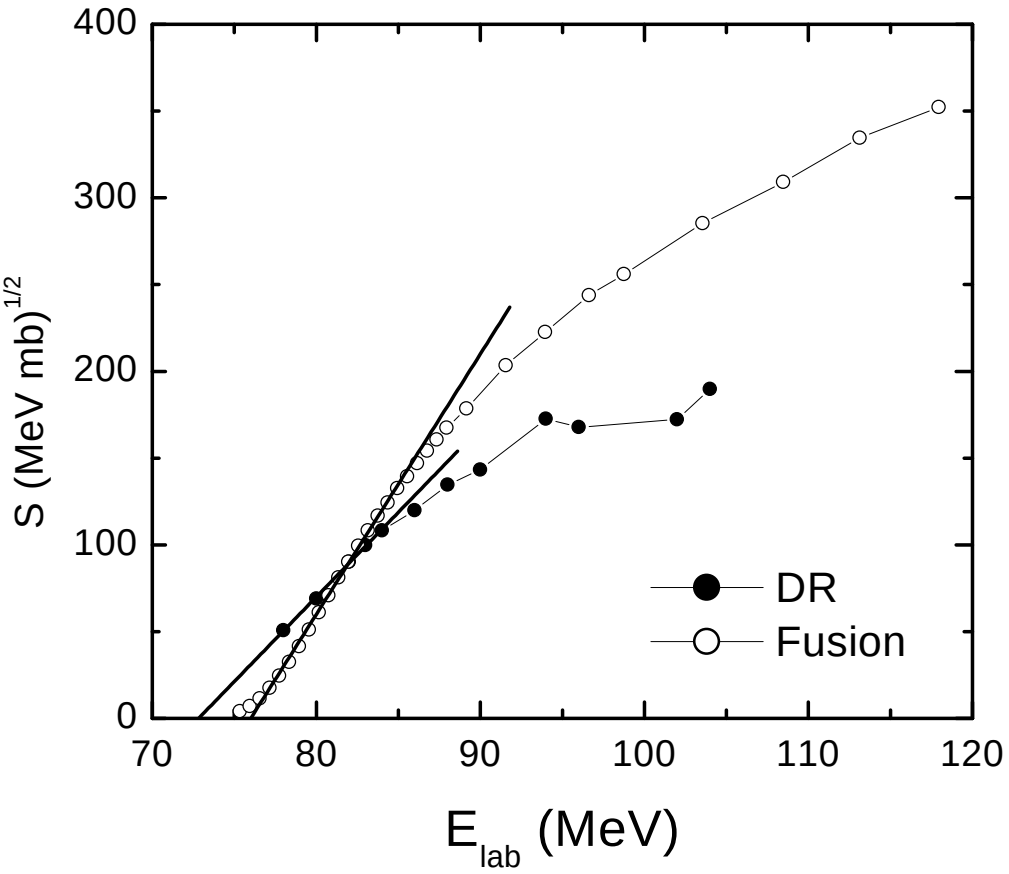
400
300
200
100
0
70
80
90
100
110
120
S (MeV mb)^1/2
E_lab (MeV)
DR
Fusion

Fig. 4

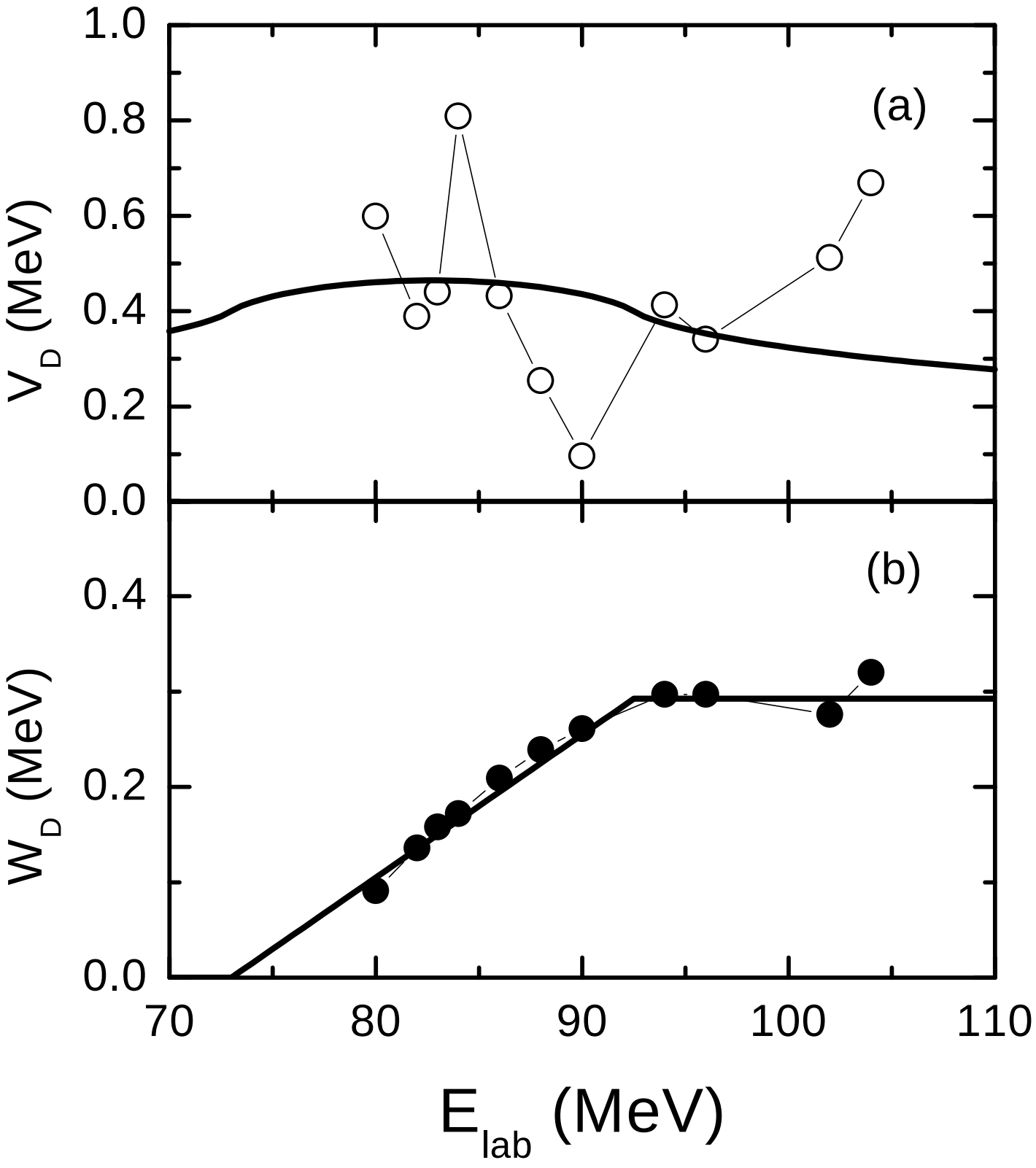

Fig. 5

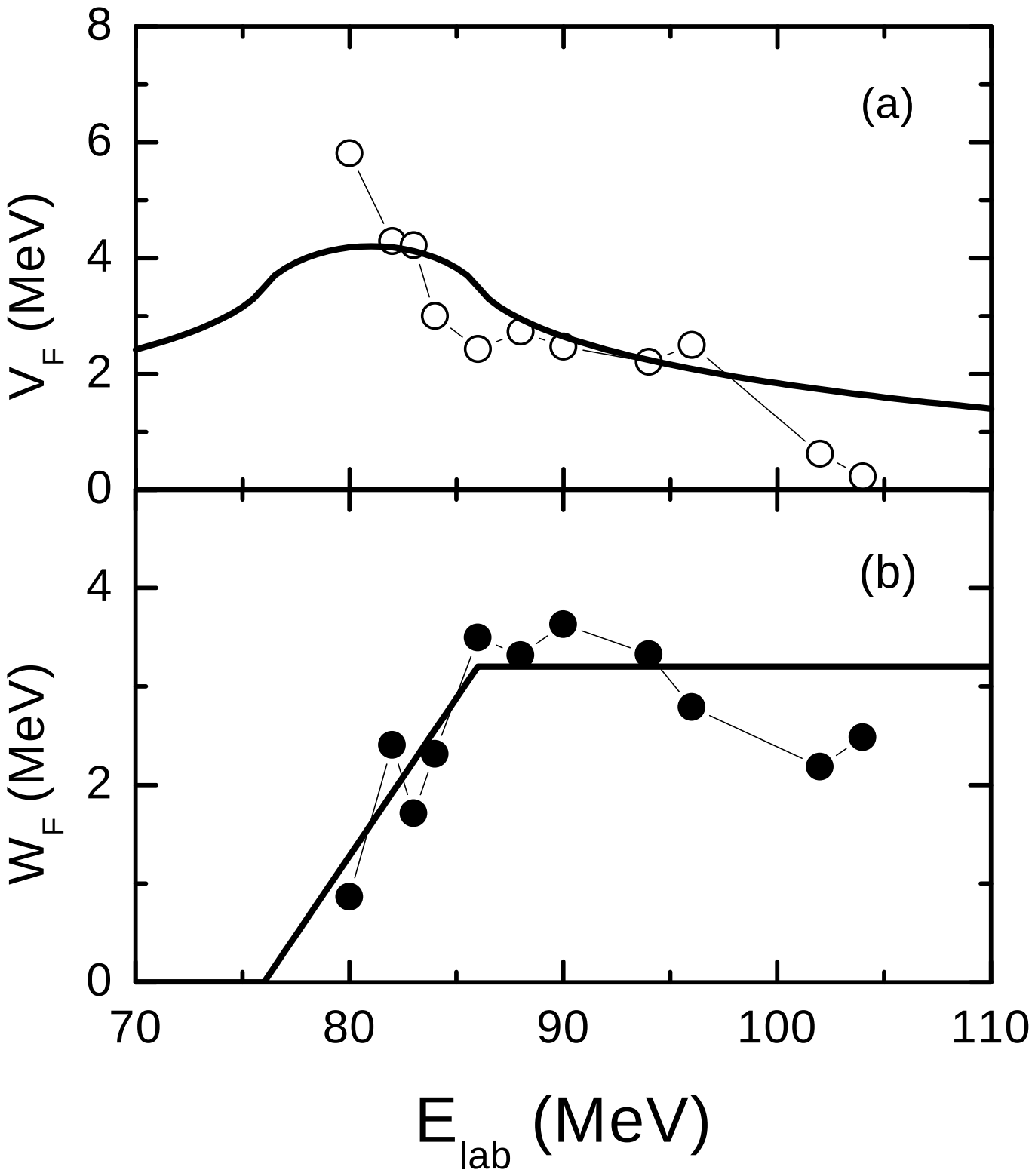

Fig. 6

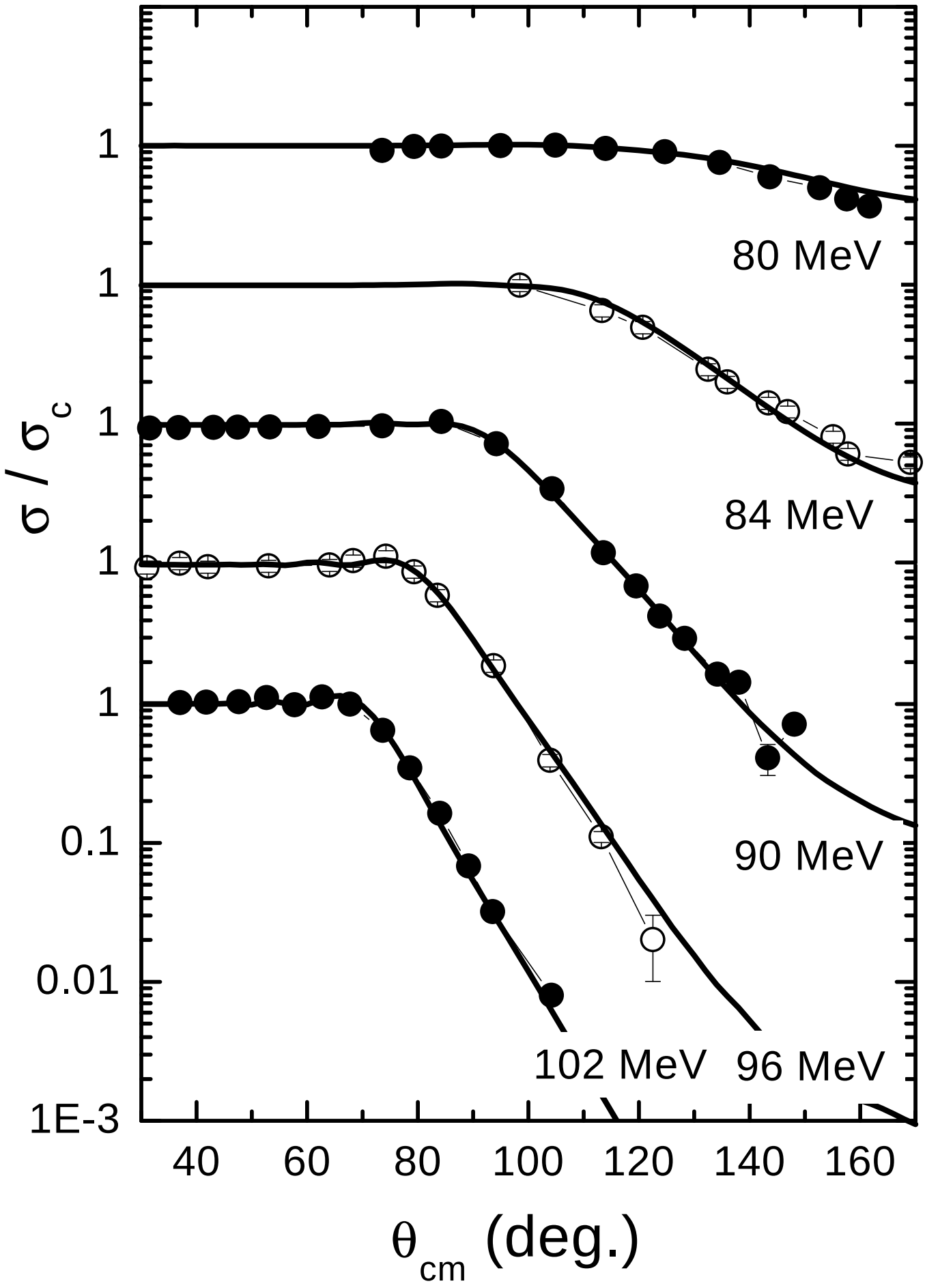
1
1
1
1
1
0.1
0.01
1E-3
σ / σc
80 MeV
84 MeV
90 MeV
96 MeV
102 MeV
40
60
80
100
120
140
160
θcm (deg.)

Fig. 7

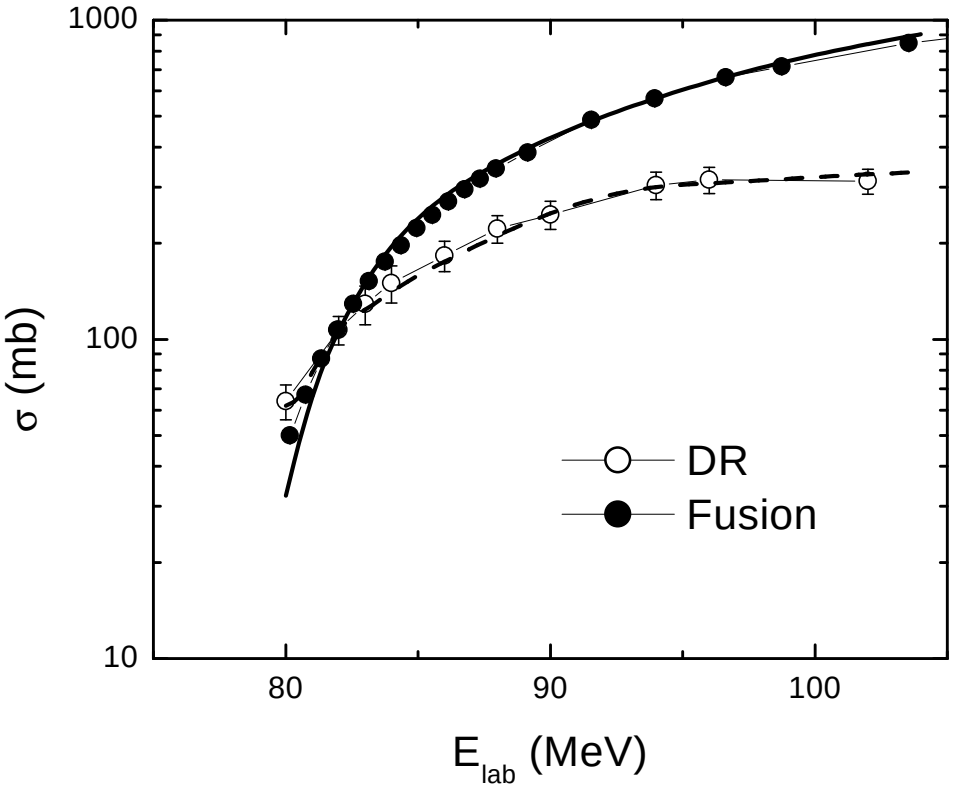

Fig. 8